Nitrogen diffusion in doped TiO_2 (110) single crystals: a combined XPS and SIMS study

Robert G. Palgrave,* David J. Payne and Russell G. Egdell

Received 6th July 2009, Accepted 24th August 2009
First published as an Advance Article on the web 1st October 2009
DOI: 10.1039/b913267h

Rutile TiO_2 (110) single crystals were doped with nitrogen by heating at 675 °C in flowing NH_3 gas. This caused a red shift in the band edge and an increase in visible region absorption. Nitrogen depth profiles obtained using dynamic secondary ion mass spectrometry (SIMS) could best be fitted by assigning three distinct diffusion coefficients. X-Ray photoelectron spectroscopy (XPS) indicated the presence of two surface nitrogen states with binding energies of 395.6 eV (substitutional N) and 399.8 eV (interstitial N). Angle resolved XPS measurements allowed us to link the XPS environments to the SIMS diffusion profiles. Subsequent air annealing at 500 °C led to asymmetric diffusion of the interstitial nitrogen into the bulk, removal of substitutional nitrogen into the gas phase, a decrease in the concentration of Ti^{3+} and a blue shift in the band edge. These changes could be related to variation in the optical band gap, and it was found that the principle cause of band gap narrowing was substitutional rather than interstitial nitrogen.

Introduction

Nitrogen doped TiO_2 is a promising material for catalysis of visible light photochemical reactions, including mineralisation of harmful pollutants[1–5] and hydrogen production from water or hydrocarbons.[6] Photocatalysis involves photoexcitation of a valence band electron into the conduction band. The resulting excited electron and hole then go on to participate in redox reactions on surface adsorbed molecules.[7] Since photoexcitation of the semiconductor is the key step in this process, the magnitude of the band gap is critical in determining the photon energy necessary to induce photoactivity. Despite the apparent success in fabricating visible light active photocatalyst materials by nitrogen doping, the precise cause of the visible light response and the exact nature of the active nitrogen dopants have not been widely agreed upon, as highlighted by Thompson and Yates in their recent review.[8]

It has been found in several experimental and theoretical studies that in both common polymorphs of TiO_2 (anatase and rutile) nitrogen doping introduces filled N 2p states above the TiO_2 valence band maximum.[1,9,10] Thus, nitrogen doping causes band gap narrowing, and shifts the photocatalytic response of TiO_2 towards the visible region. However, there are some reports to the contrary, *i.e.* band gap widening has been claimed to result from N doping, especially in the rutile phase,[11–14] and as such this remains a contentious issue. A complicating factor is that different forms of nitrogen dopant are known: nitrogen substituting for a lattice oxide anion, N_O, and interstitial nitrogen atoms or molecules, N_i, as well as other forms, are commonly reported, although their presence depends heavily upon the fabrication method used.[1,9,15–22] It remains a key question to determine the effect of each of these nitrogen species on the electronic structure and photocatalytic properties of the material. A second problematic area is that of the concentration of N dopants. The low nitrogen dopant levels typically reported in these studies would imply that the N 2p states are localised. However, it has been found that visible light generated holes, which are presumably located on these N 2p states, are mobile enough to participate in surface redox chemistry, and hence cause visible light photocatalysis.[22]

Difficulties in adequately characterising and understanding the influence of dopants in polycrystalline samples of N doped TiO_2 have hampered attempts to resolve these and other issues. This has led some researchers to study the doping of single crystals of TiO_2,[19,23] or of epitaxial TiO_2 films grown by molecular beam epitaxy.[9,20–22] Such systems offer structural simplicity and allow stronger conclusions to be drawn on structure–function relationships. In this vein, here we report a combined surface and bulk study of N doped TiO_2 single crystals using X-ray photoelectron spectroscopy (XPS) and dynamic secondary ion mass spectrometry (SIMS). While SIMS has previously been used to observe the depth profiles of ion implanted nitrogen in TiO_2,[23] in this study we focus in detail on nitrogen diffusion processes in N doped TiO_2 upon oxidation and reduction. Furthermore, we have employed angle resolved XPS measurements to link chemical environment information to the components of the SIMS diffusion profiles, which has allowed us to determine the diffusion behaviour of different N species. Finally, by measuring changes to the band gap through UV/visible absorption spectroscopy, we have assessed the contribution to band gap narrowing of substitutional and interstitial nitrogen dopants.

Experimental section

Commercial epi-polished rutile single crystals (PiKem Ltd.) were cleaned ultrasonically in acetone, propan-2-ol, and Millipore water. They were then heated in recrystallised alumina boats to temperatures from 550 to 675 °C in air, and exposed to NH_3 gas with a flow rate of 200 cm^3 min^{-1} for periods of time up to 80 min.

University of Oxford, Chemistry Research Laboratory, Mansfield Road, Oxford, UK OX1 3TA. E-mail: robert.palgrave@chem.ox.ac.uk

After the required time had elapsed, samples were withdrawn from the furnace at high temperature and cooled rapidly (<1 min) to room temperature in air by placing on a metal surface. This quenching step was found to be essential to obtain repeatable results as will be described *infra*. Subsequent oxidation was carried out by annealing samples in air at 500 °C. Subsequent reduction was carried out by annealing samples at 750 °C in an ultra high vacuum chamber with a base pressure of 10^{-9} mbar.

High resolution X-ray photoemission spectra (XPS) were recorded in a Scienta ESCA 300 spectrometer located at Daresbury Laboratory, UK, which incorporated a rotating anode Al K_α ($h\nu = 1486.6$ eV) X-ray source. The X-ray source was run with 200 mA emission current and 14 kV anode bias, while the analyser operated at 150 eV pass energy with 0.8 mm slits. Gaussian convolution of the analyser resolution with a line width of 260 meV for the monochromated X-ray source gives an effective instrument resolution of 400 meV.

Secondary ion mass spectrometry (SIMS) was carried out using a Cameca IMS 3f SIMS instrument located at Loughborough Surface Analysis Ltd. A 14.5 kV Cs^+ primary ion beam was used and negative secondary ions were measured. Titanium depth profiles were measured as the matrix standard using the anion of the principle isotope (^{48}Ti). Since it is not possible to detect N^- due to the negative electron affinity of N, nitrogen profiles were measured using the $^{16}O^{14}N$ anionic fragment. $^{48}Ti^{14}N$ is unsuitable for quantification of N concentrations due to interference from $^{46}Ti^{16}O$ whilst $^{46}Ti^{14}N$ gave a very low ion yield. After SIMS analysis the crater depths were measured with a Dektak 6M profilometer in order to produce an absolute depth scale.

UV/visible absorption spectra were measured using an SLS Libra S6 spectrometer. All optical spectra were taken with the sample at room temperature.

Results

UV/visible spectroscopy

The UV/visible absorption spectrum of a rutile TiO_2 single crystal is typical of a wide band gap semiconductor. There is a region of strong absorption at photon energies above the band gap energy and low absorption throughout the remainder of the visible region. The fundamental interband transition is direct,[24] and its energy can be obtained from the absorption edge using Tauc's method.[25] The band gap of undoped TiO_2 was measured in this way as 2.98 eV, in good agreement with the widely established value of 3.06 eV.

TiO_2 crystals were heated for 80 min in flowing ammonia gas (flow rate 0.2 L min^{-1}) at 550 °C, 600 °C and 675 °C. Heating in ammonia induced two changes in the spectrum, as shown in Fig. 1. Firstly, there is an increase in absorption in the visible region and toward the infrared cutoff of the spectrometer at 800 nm, corresponding to the presence of Ti^{3+}, *i.e.* the reduction of TiO_2.[26] Greater visible region absorption was observed at higher annealing temperatures, indicating a greater degree of reduction. Secondly, there was a small red shift in the absorption edge. This band gap narrowing increased with increasing annealing temperature, the greatest change being seen in the sample annealed at 675 °C, in which the Tauc optical band gap fell to 2.94 eV. The narrowing of the band gap has been previously assigned to the presence of N 2p states above the TiO_2 valence band maximum.[9,27]

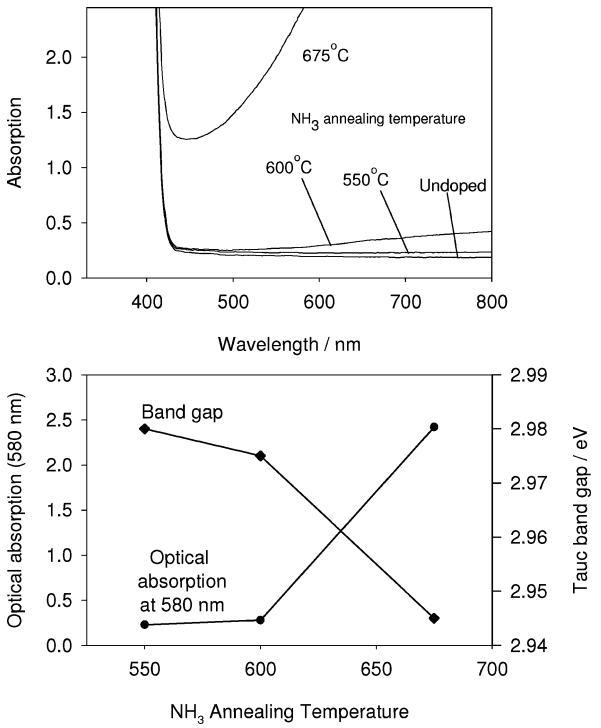

Fig. 1 Top panel: UV/vis spectra of TiO_2 (110) single crystals undoped and annealed in NH_3 at 550–675 °C for 80 min. Bottom panel: variation in optical absorption intensity at $\lambda = 580$ nm (circles) and Tauc band gap (diamonds) with annealing temperature.

Subsequent oxidation experiments were carried out on the sample annealed in ammonia at 675 °C. The sample was annealed in air at 500 °C, and this treatment led to a decrease in the visible region optical absorption, signifying the oxidation of Ti^{3+} back to Ti^{4+} (Fig. 2). Initially there was a further red shift of the band gap, reaching a minimum of 2.91 eV, and then on yet further annealing a blue shift of the band gap was observed, reaching a maximum of 2.97 eV. This is close to the band gap of the original undoped crystal.

X-Ray photoelectron spectroscopy (XPS)

Photoelectron spectra were taken on the sample annealed in ammonia at 675 °C for 80 min and again on the same sample after a subsequent 10 min of air annealing at 500 °C. In order to probe the depth distribution of the nitrogen species, X-ray photoelectron spectra were taken using normal emission geometry (90° take off angle) and grazing emission geometry (10° take off angle). Spectra taken at grazing emission angles have a shallower sampling depth, as the photoelectron escape distance is $d(\sin\theta)$, where d is the sampling depth at normal emission and θ is the take off angle. Thus by taking spectra at different emission angles, depth profile information can be obtained.

The N 1s core lines recorded at 90° and 10° are shown in Fig. 3. The spectra are fitted with Voigt functions and are normalised to the Ti $2p_{3/2}$ core line; the O 1s core line was not used for

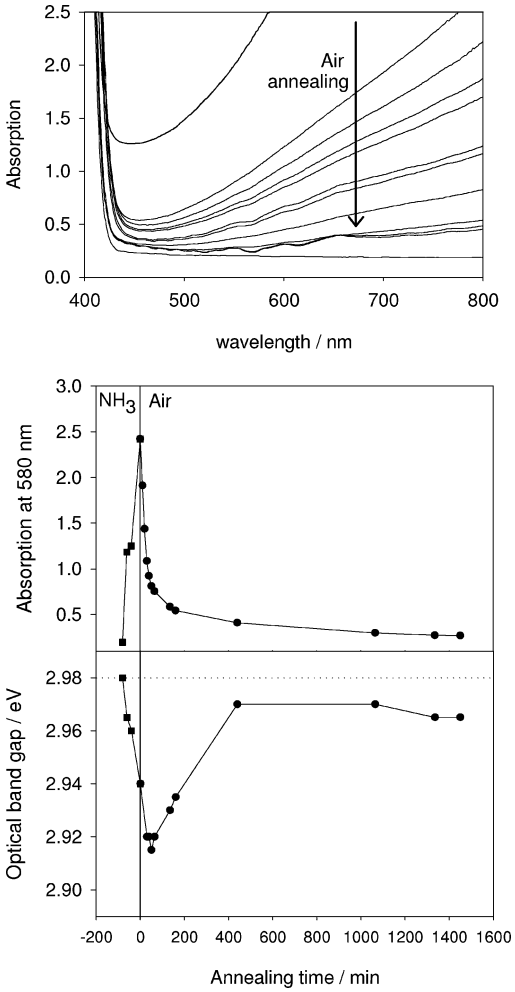

Fig. 2 Top panel: UV/vis spectra of a TiO_2 (110) single crystal annealed in NH_3 at 675 °C for 80 min (top spectrum) and subsequently annealed in air (lower spectra). Middle panel: changes in the visible light absorption intensity at $\lambda = 580$ nm. Bottom panel: Tauc band gap of a TiO_2 (110) crystal annealed in NH_3 at 675 °C ($t < 0$) and subsequently in air ($t > 0$). Dotted line shows the band gap of the undoped TiO_2 single crystal.

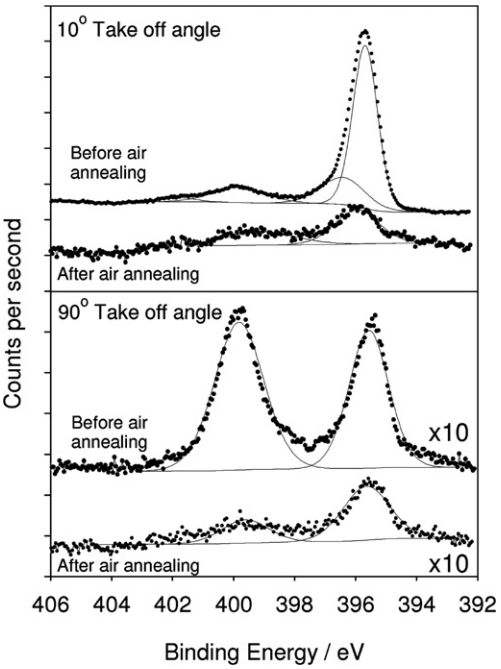

Fig. 3 X-Ray photoemission spectra of the N 1s core line taken before and after the air annealing step at take off angles of 10° (top panel) and 90° (bottom panel). For comparison, spectra are normalised to the Ti $2p_{3/2}$ core line (not shown). Data are shown as points and curve fittings, discussed in the text, are shown as solid lines.

normalisation as substitutional doping of N for O is possible.[19] Before the air annealing step, two N 1s components are observed at a 90° take off angle, with binding energies of 399.8 eV and 395.6 eV and relative peak areas 1.3 : 1. At 10° take off angle, four components are observed, with binding energies of 401.8 eV, 399.8 eV, 396.3 eV and 395.6 eV and relative area ratio 1 : 8 : 12 : 38. The enhancement of the peak area of the component at 395.6 eV compared to that at 399.8 eV in the grazing angle spectrum signifies that the N environment associated with the 395.6 eV peak is more confined to the region very near to the surface. The appearance of the 401.8 eV and 396.3 eV peaks only in the grazing angle spectrum shows that these environments are highly confined to the surface, and are possibly surface adsorbed species. After air annealing, the spectrum taken at both 90° and 10° take off angle showed that the peak at 399.8 eV had almost entirely vanished, and there was also reduction in intensity in the peak at 395.6 eV. A peak at 396.3 eV was not detected after air annealing.

The identity of the N environment associated with a N 1s peak at 397.1–395.6 eV is widely regarded as substitutional nitrogen located on an oxygen lattice site (N_O).[1,9,19–22] The variation in binding energy within this range can be explained by variation in the oxygen to nitrogen ratio, with the N 1s peak appearing at 397.1 eV in TiN,[28,29] and shifting to lower binding energies with greater oxidation.[29–31] Therefore, we assign our observed peak at 395.6 eV to substitutional nitrogen, and it is this environment that is the more surface confined. By comparison of the N 1s (395.6 eV) and O 1s peak areas, adjusted with suitable sensitivity factors, the proportion of lattice anion sites occupied by substitutional N was calculated. Using the spectra taken at 90° take off angle it was found that 0.8% of lattice anion sites were occupied by N. Using the spectra taken at 10° take off angle, which are considerably more surface sensitive, it was calculated that 5.5% of the lattice anions sites were occupied by N.

Environments with N 1s binding energies from 399–401 eV have been variously ascribed to surface adsorbed NO,[32] bulk interstitial NO^{2-},[33] interstitial N_2,[20] and interstitial N.[16–18] Perhaps most relevant to this study, Diwald *et al.* observed a N 1s peak at 399.6 eV when they similarly treated TiO_2 (110) with NH_3, and they assigned this environment to interstitial NH_x.[19] Our observed peak at 399.8 eV is very likely to be of the same origin, although we have no evidence for or against the presence of N–H bonds. We will denote the interstitial nitrogen species corresponding to our observed peak at 399.8 eV as N_i, without making a specific claim as to its exact nature at this stage. The environment with a N 1s binding energy of 396.3 eV is highly surface confined, and is most likely a surface adsorbed species. It matches closely with chemisorbed atomic N, reported with N 1s

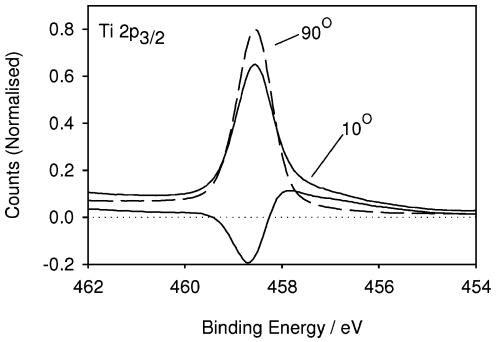

Fig. 4 X-Ray photoemission spectra of the Ti $2p_{3/2}$ core line recorded at take off angles of 10° (solid line) and 90° (dashed line). The peaks are normalised to the sum of the O 1s and N 1s (395.6 eV) peaks, and the difference is shown by the lower solid line.

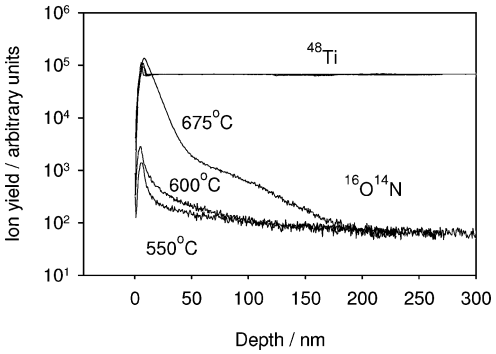

Fig. 5 Dynamic SIMS depth profiles of TiO_2 single crystals annealed in NH_3 for 80 min at 550 °C, 600 °C and 675 °C. The $^{16}O^{14}N$ ion intensity varies with depth. The ^{48}Ti ion intensity is invariant after 3 nm of etching.

binding energy of 396 eV, or possibly strongly chemisorbed N_2, reported with a binding energy of 397.5 eV.[29,34] Similarly, the environment with a N 1s binding energy of 401.8 eV is also likely to be surface adsorbed, and its binding energy greater than that found in elemental N (400 eV) suggests that it corresponds to a NO_x species, possibly adsorbed NO.[15]

The Ti $2p_{3/2}$ core lines recorded at 90° and 10° are shown in Fig. 4. The spectra are normalised to the sum of the O 1s and the N 1s (395.6 eV) peaks—*i.e.* the lattice anions—accounting for atomic sensitivity factors. At 90° emission the spectrum can be fitted with a single peak at 458.6 eV corresponding to Ti^{4+}. At 10° emission, a shoulder on the low binding energy side of the peak is clearly visible, and it can be seen from the difference spectrum that intensity has been transferred from the main peak at 458.6 eV to this shoulder. This feature has been assigned previously by our group and others as Ti^{4+} octahedrally surrounded by a combination of O_O and N_O lattice anions.[9,10] This result reinforces the conclusion that N_O is the more surface segregated nitrogen species, as Ti bonded to N_O is seen only in the grazing angle photoemission spectrum.

Secondary ion mass spectrometry (SIMS)

Dynamic SIMS depth profiles of the TiO_2 crystals treated with ammonia at 550 °C, 600 °C and 675 °C are shown in Fig. 5. Increasing amounts of N are present with increasing NH_3 annealing temperature, in accordance with the UV/visible spectroscopy results. In each case, the $^{16}O^{14}N$ signal decreased with increasing depth, reaching what appeared to be a baseline of around 10^2 counts. The nitrogen diffusion profile of the TiO_2 crystal treated in ammonia at 675 °C for 80 min (shown in Fig. 5) was fitted using the following procedure (shown in Fig. 6). The $^{16}O^{14}N$ signal was normalised to the ^{48}Ti matrix, which is invariant after approximately 3 nm of etching. The initial variation in ^{48}Ti represents a region of surface contamination on the samples which had been handled and stored in air. The diffusion of a thin film into a semi-infinite substrate is described by a solution of Fick's law:[35]

$$c(x,t) = c_0 \mathrm{erfc}\left(\frac{x}{2\sqrt{Dt}}\right) \quad (1)$$

where $c(x, t)$ is the species concentration at depth x and time t, c_0 is the concentration at the surface at $t = 0$, and D is the diffusion

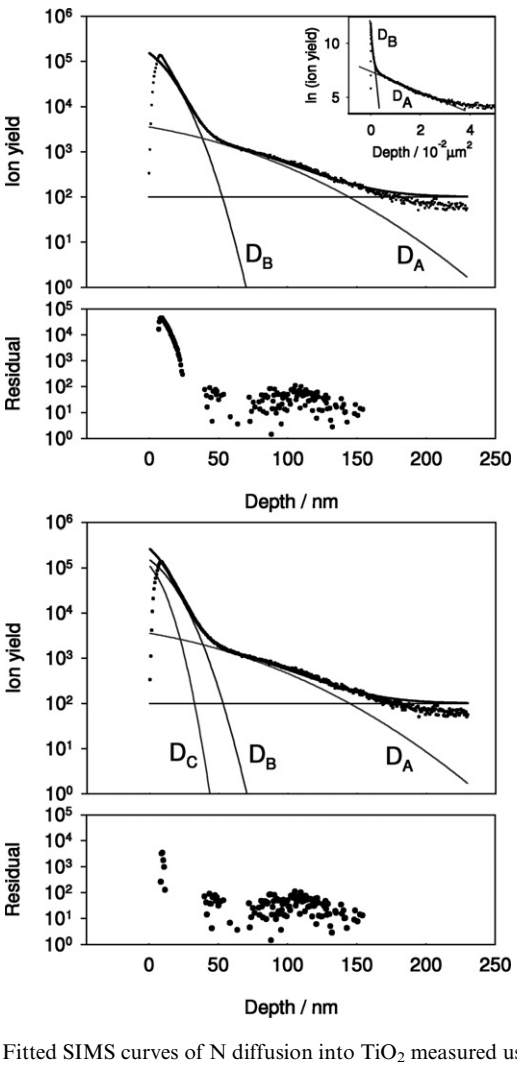

Fig. 6 Fitted SIMS curves of N diffusion into TiO_2 measured using the $^{16}O^{14}N$ fragment normalised to the matrix ^{48}Ti signal. Top panels show experimental diffusion profile (points) fitted with two diffusion profiles (D_A and D_B, solid lines), and a constant background component, with the resulting sum also shown. The diffusion coefficients for D_A and D_B were obtained from the inset diffusion plot. The residual shows the presence of a third diffusion profile (D_C), which is added to the fit in the bottom panels, giving excellent agreement with the experimental data.

coefficient. The function erfc(x) is the complimentary error function of x. A diffusion plot of x^2 *vs.* ln(ion yield) is typically used to determine diffusion coefficients, and such a plot reveals two distinct straight line segments (inset, Fig. 6), with diffusion coefficients calculated from the line gradients as $D_A = 4.50 \times 10^{-7}$ μm^2 s^{-1} and $D_B = 2.53 \times 10^{-8}$ μm^2 s^{-1}. These two values were used to model diffusion curves using eqn (1), and these were fitted to the experimental diffusion profile, with an additional constant baseline of 10^2 counts, and the fit optimised through a least squares method as shown in Fig. 4. The residual plot distinctly shows the presence of a third diffusion profile, which was duly added to the model and optimised, and found to have the diffusion coefficient $D_C = 9.50 \times 10^{-9}$ μm^2 s^{-1}. The components of the diffusion profile with coefficients D_A, D_B and D_C as given above will be referred to as components A, B, and C, respectively.

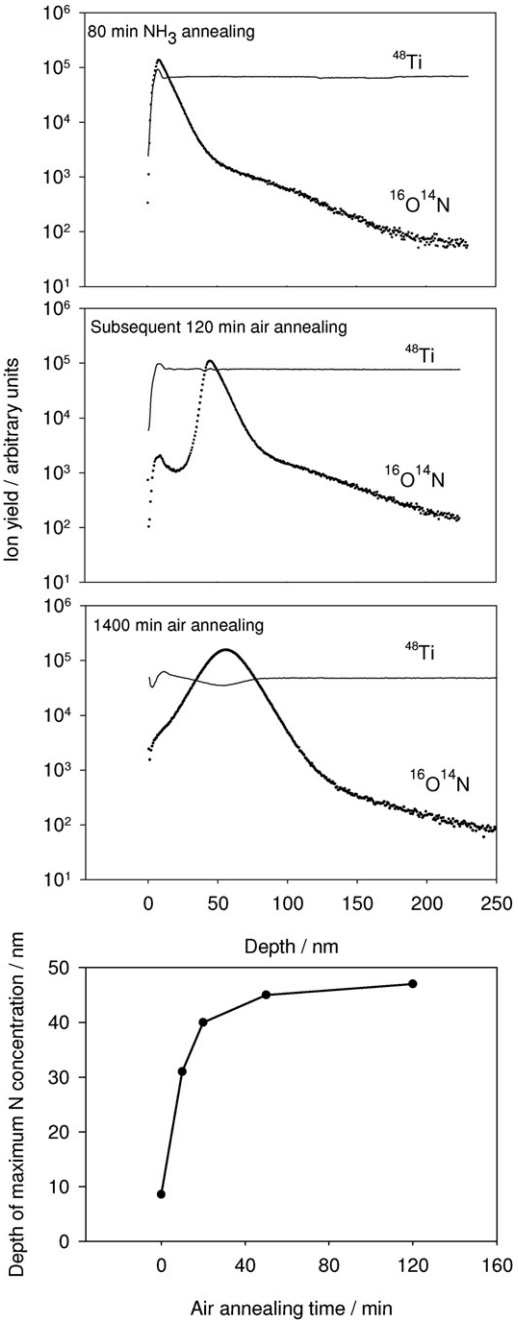

Fig. 7 SIMS depth profiles of N diffusion into TiO_2 (110). Depth profiles are shown after 80 min of annealing in NH_3 (top panel) and after subsequent 120 min and 1400 min of annealing in air (second and third panel). Two components of the nitrogen depth profile (identified as N_i, see text) migrate from the surface to the bulk during this treatment. One component (identified as N_O, see text) remains at the surface and decreases in intensity, and is undetected at the longest annealing time. The matrix signal from ^{48}Ti is unchanged. Bottom panel: the change in the depth of the N concentration maximum upon air annealing up to 120 min.

Annealing the sample in air at 500 °C in steps of 10 min and repeating SIMS analysis after each step revealed a striking change in the nitrogen depth profile, shown in Fig. 7. A significant fraction of the N dopant derived from the components A and B migrated from the surface into the bulk, to give a concentration maximum no longer located at the surface. The depth of the N concentration maximum increased with increasing air annealing time, reaching a depth of 47 nm after 120 min of air annealing. A small local maximum of N concentration remained at the surface, which could correspond to component C, although the intensity of the N signal had lessened significantly, perhaps due to escape of the N containing species from the surface. After 1400 min of air annealing, the depth of the nitrogen concentration maximum increased to 59 nm. The intensity of this SIMS peak had not decreased appreciably from that observed immediately after NH_3 annealing, but had broadened slightly. The local maximum at the surface, corresponding to component C, was not observed after 1400 min of air annealing. Throughout annealing, the ^{48}Ti matrix signal remained unchanged within instrumental error.

Discussion

The diffusion profiles measured by SIMS and their behaviour after air annealing can be matched to the nitrogen environments observed by XPS. There are two N main environments observed in XPS, corresponding to substitutional N, denoted N_O, and some form of interstitial N, denoted N_i. A third and fourth environment, seen at binding energies of 401.8 eV and 396.3 eV, are highly localised at the surface and match very well with surface adsorbed species, so we can disregard these components in the discussion of diffusion in the bulk material. It was observed by XPS that prior to air annealing, N_O was more surface confined than N_i, and that after air annealing, the intensity of the N_i environment was reduced to almost zero, whereas the N_O environment was also reduced in intensity, but a measurable amount remained. From this information, N_O can be matched to the SIMS component C. This component having the smallest diffusion coefficient ($D_C = 9.50 \times 10^{-9}$ μm^2 s^{-1}) is the most surface confined. On air annealing, this component remains on the surface, unlike components A and B, but reduces in intensity. This is exactly the behaviour of the N_O peak seen in the photoelectron spectra. Components A and B are therefore assigned as N_i, as these are less surface confined (have greater diffusion coefficients) than N_O, and diffuse into the bulk on air annealing, beyond the probing depth of XPS analysis (around 10 nm), and so vanish from the photoelectron spectra. The fact that

both components A and B are affected in the same way by air annealing supports their joint assignment as N_i, but the question remains as to why two separate diffusion coefficients, D_A and D_B, are observed. As annealing of TiO_2 single crystals creates a disordered surface region,[12] these two coefficients could correspond to slower volume diffusion and faster grain boundary diffusion.[36] This would imply that the disordered region created by the NH_3 annealing process is at least 200 nm in thickness, since this is the depth to which the grain boundary diffusion profile penetrates.

It is not possible to obtain an internal (*i.e.* non-surface) concentration maximum for a species diffusing from the surface along a concentration gradient as described by Fick's law, and so a more complex mechanism for N_i diffusion must be at work. The observation that the surface to bulk diffusion of N_i occurred on annealing in air at 500 °C but did not occur during annealing in ammonia at 675 °C points to a mechanism driven by surface oxidation. In order to investigate this process further, a sample which had been air annealed for 120 min and had a N concentration maximum at a depth of 47 nm was reduced by annealing in ultra high vacuum (10^{-9} mbar) at 750 °C for 1 h. The objective of this treatment was to cause surface reduction of TiO_2.[37,38] The SIMS depth profile of the sample after reduction (Fig. 8) showed that the depth of the N concentration maximum had decreased to 41 nm, *i.e.* N_i had diffused back towards the surface upon reduction.

It has therefore been established that N_i diffuses into the bulk upon surface oxidation and diffuses towards the surface upon surface reduction. The nature of the nitrogen defects in N doped TiO_2 will now be considered, followed by a discussion of the possible causes for their diffusion behaviour. Electron paramagnetic resonance measurements have shown that N_i and N_O defects in TiO_2 are largely diamagnetic.[13,14] This implies that N_O must carry a 3− charge, since N^{2-} and N^{-} are both paramagnetic. If N_i exists as a monatomic ion, then it too must bear a 3− charge in order to be diamagnetic. However, Di Valentin *et al.* have found through theoretical treatments that N_i within rutile channels closely binds to lattice oxygen, and they suggest that N_i might be described as NO molecules on oxygen lattice sites, here denoted $(NO)_O$.[11] In this case the requirement for diamagnetism

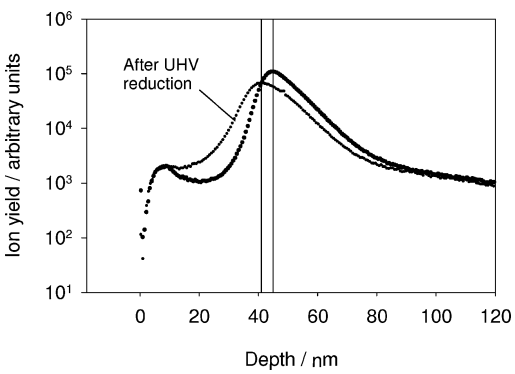

Fig. 8 SIMS $^{16}O^{14}N$ depth profile showing N diffusion into TiO_2 (110) after 120 min of air annealing and after subsequent reduction by annealing in ultra high vacuum at 750 °C for 1 h. Vertical lines show the depths of the concentration maxima. The reduction causes migration of N_i from the bulk towards the surface.

means that $(NO)_O$ should carry a 3− charge, as NO^{2-} and NO^{-} are paramagnetic. Using Kroger–Vink notation, the diamagnetic substitutional nitrogen defect can be written as N'_O while the monatomic interstitial nitrogen defect is N'''_i and the alternative diatomic form is $(NO)'_O$. The principle native point defects found in reduced TiO_{2-x} are Ti'_{Ti}, $V_O^{\bullet\bullet}$ and $Ti_i^{\bullet\bullet\bullet}$.[35,37–40] Of the native cationic defects, at equilibrium and at experimentally attainable partial pressures of oxygen, $V_O^{\bullet\bullet}$ is significantly more abundant than $Ti_i^{\bullet\bullet\bullet}$, although the latter is known to be more mobile, and is primarily responsible for the bulk assisted oxidation of surface reduced TiO_2 *in vacuo*.[37] The stoichiometries of nitrogen doped TiO_2 can be stated by balancing defect charges. Assuming the concentration of $Ti_i^{\bullet\bullet\bullet}$ to be small, charge neutrality requires that:

$$2[V_O^{\bullet\bullet}] = [N'_O] + 3[N'''_i] + [Ti'_{Ti}] \quad (2)$$

for the case of a monatomic N_i defect, or if Di Valentin's model is used for the interstitial nitrogen defect:

$$2[V_O^{\bullet\bullet}] = [N'_O] + [(NO)'_O] + [Ti'_{Ti}] \quad (3)$$

Thus if the overall stoichiometry of the material is expressed as $TiO_{2-x}(N_O)_y(N_i)_z$ then:

$$x \geq \frac{3}{2}(y+z) \quad (4)$$

for the case of a monatomic N_i defect. The inequality in the above equation arises due to the possible presence of Ti'_{Ti}. Using Di Valentin's model of a diatomic interstitial nitrogen defect, the relation becomes:

$$x \geq \frac{3}{2}y + \frac{1}{2}z \quad (5)$$

The oxidation of bulk reduced TiO_2 in air represents the movement of $Ti_i^{\bullet\bullet\bullet}$ and $V_O^{\bullet\bullet}$ from the bulk to the surface where they are consumed, while the reduction of TiO_2 represents the movement of these defects in the opposite direction.[41,42] The diffusion of anionic nitrogen defects into the bulk upon oxidation in air may be due to the surface region becoming depleted of cationic defects ($Ti_i^{\bullet\bullet\bullet}$, $V_O^{\bullet\bullet}$) making diffusion of nitrogen into the bulk favourable through electrostatic attraction. Under this hypothesis, it would be assumed that N'_O, which is observed to remain on the surface, is incapable of diffusing to the bulk in the same way as interstitial nitrogen as it is less mobile.

Alternatively, it is possible that movement of either $Ti_i^{\bullet\bullet\bullet}$ or $V_O^{\bullet\bullet}$ becomes correlated with the movement of N_i to the bulk, *i.e.* there is cooperative movement of N_i and native TiO_2 defects in opposite directions. Such a mechanism has been proposed by Sanz *et al.*, who recently carried out a DFT study on N doped rutile TiO_2 and suggested that diffusion of V_O from the bulk to the surface may occur synchronously with the diffusion of N_O to the bulk.[18] In fact we have found that it is N_i that undergoes surface to bulk diffusion. If interstitial nitrogen is considered as $(NO)_O$ then it can be seen that cooperative diffusion of V_O and $(NO)_O$ through the vacancy mechanism might occur, however, a new question then arises: why does N'_O not also diffuse *via* this mechanism, instead of remaining on the surface as observed experimentally? It is perhaps more likely that diffusion of N_i is

correlated with that of the mobile $Ti_i^{\bullet\bullet\bullet}$ defect, although further study is required before a definitive answer can be given.

The decrease in both the XPS and the SIMS signals associated with N_O with air annealing points to the removal of N_O from the surface, probably as gaseous NO_x species; it has been calculated that substitutional N is thermodynamically unstable with respect to removal into the gas phase in this way, and also that N_i is more stable than N_O under oxygen rich conditions.[11] It is unknown from this work whether N_i is stable with respect to removal into the gas phase, or whether its removal is prevented by its diffusion to the bulk.

In the light of the above discussion, the changes in the band gap, which is critical to photocatalytic performance, can be considered. We found that the band gap falls on annealing in ammonia, and we attribute this to creation of filled N 2p derived states above the top of the valence band in agreement with others.[9,27] However, there are some experimental and theoretical reports of the band gap of rutile TiO_2 increasing on N doping,[12–14] and this is at odds with our findings. However, the decreases in band gap that we have measured are small, and the concentration of nitrogen in the samples reported here is greater than in some of these other works. On air annealing, the band gap falls further during the first 20 min, before increasing again and plateauing after 400 min at 2.97 eV, 0.01 eV below the value measured for the undoped crystal. Thus after long periods of air annealing, the absorption spectrum of the samples was very similar to undoped TiO_2. However, it is known from the SIMS data (Fig. 7) that a significant amount of N_i is present in the bulk even after 1400 min of air annealing, while N_O is removed into the gas phase by air annealing. It can therefore be stated that the presence of bulk N_i has very little effect on the band gap of rutile TiO_2, causing a negligible band gap decrease, around 0.01 eV. This strongly suggests that the band gap narrowing observed is due almost entirely to N_O, as has been suggested by others.[9,23] The increase in the band gap on extended air annealing can thus be satisfactorily explained by the loss of N_O from the surface, which was observed by both XPS and SIMS. The total band gap decrease caused by N_O was determined to be 0.06 eV, and it can thus be concluded that the N_O derived electronic states are situated around 0.06 eV above the TiO_2 valence band maximum. Furthermore, the slight initial decrease in the band gap at the start of the air annealing procedure might be associated with spatial separation of the N_i and N_O dopants.

Conclusions

Through a combined SIMS and XPS study, bulk diffusion phenomena in N doped TiO_2 (110) have been studied. As observed by XPS, two N containing species are present in N doped TiO_2 produced by annealing in NH_3. Following Diwald *et al.*[19] and others, we have assigned these environments as substitutional and interstitial nitrogen. Using dynamic SIMS we observed a surface to bulk diffusion of the interstitial nitrogen species, N_i, upon oxidation of the sample, and the reverse movement upon subsequent reduction. Meanwhile, on heating in air the substitutional dopant, N_O, was removed into the gas phase. The identification of the species of N dopant allowed their contribution to the band gap narrowing to be determined. The presence of bulk N_i has very little effect on the band gap of rutile TiO_2, and this leads to the conclusion that N_O is the cause of the band gap reduction which is crucial for visible light photocatalysis. The unusual and differing diffusion behaviour of two types of N dopant means that the precise method used for sample preparation and processing might have a significant effect on the dopant distribution, and thus thermal history of a sample may heavily impact photocatalytic performance. This may go some way to explaining the difficulties thus far in ascertaining the exact role of the N dopant in visible light photocatalysis.

Acknowledgements

The work in Oxford was supported by European Union grant NATAMA (NMP3-CT-2006-032583). The NCESS facility at Daresbury Laboratory is supported by EPSRC grant EP/E025722/1. The authors thank Loughborough Surface Analysis Ltd. for SIMS analysis.

Notes and references

1 R. Asahi, T. Morikawa, T. Ohwaki, K. Aoki and Y. Taga, *Science*, 2001, **293**, 269–271.
2 W. Balcerski, S. Y. Ryu and M. R. Hoffmann, *J. Phys. Chem. C*, 2007, **111**, 15357–15362.
3 H. Choi, M. G. Antoniou, M. Pelaez, A. A. De la Cruz, J. A. Shoemaker and D. D. Dionysiou, *Environ. Sci. Technol.*, 2007, **41**, 7530–7535.
4 D. Luca, C. M. Teodorescu, R. Apetrei, D. Macovei and D. Mardare, *Thin Solid Films*, 2007, **515**, 8605–8610.
5 U. Stafford, K. A. Gray and P. V. Kamat, *Heterog. Chem. Rev.*, 1996, **3**, 77–104.
6 T. Sreethawong, S. Laehsalee and S. Chavadej, *Catal. Commun.*, 2009, **10**, 538–543.
7 A. Mills and S. LeHunte, *J. Photochem. Photobiol., A*, 1997, **108**, 1–35.
8 T. L. Thompson and J. T. Yates, *Chem. Rev.*, 2006, **106**, 4428–4453.
9 S. A. Chambers, S. H. Cheung, V. Shutthanandan, S. Thevuthasan, M. K. Bowman and A. G. Joly, *Chem. Phys.*, 2007, **339**, 27–35.
10 I. Takahashi, D. J. Payne, R. G. Palgrave and R. G. Egdell, *Chem. Phys. Lett.*, 2008, **454**, 314–317.
11 C. Di Valentin, E. Finazzi, G. Pacchioni, A. Selloni, S. Livraghi, M. C. Paganini and E. Giamello, *Chem. Phys.*, 2007, **339**, 44–56.
12 O. Diwald, T. L. Thompson, E. G. Goralski, S. D. Walck and J. T. Yates, *J. Phys. Chem. B*, 2004, **108**, 52–57.
13 S. Livraghi, M. C. Paganini, E. Giamello, A. Selloni, C. Di Valentin and G. Pacchioni, *J. Am. Chem. Soc.*, 2006, **128**, 15666–15671.
14 C. Di Valentin, G. Pacchioni and A. Selloni, *Phys. Rev. B: Condens. Matter*, 2004, **70**, 085116-1–085116-4.
15 H. M. Yates, M. G. Nolan, D. W. Sheel and M. E. Pemble, *J. Photochem. Photobiol., A*, 2006, **179**, 213–223.
16 L. Mi, P. Xu and P. N. Wang, *Appl. Surf. Sci.*, 2008, **255**, 2574–2580.
17 C. Di Valentin, G. Pacchioni, A. Selloni, S. Livraghi and E. Giamello, *J. Phys. Chem. B*, 2005, **109**, 11414–11419.
18 J. Graciani, L. J. Alvarez, J. A. Rodriguez and J. F. Sanz, *J. Phys. Chem. C*, 2008, **112**, 2624–2631.
19 O. Diwald, T. L. Thompson, T. Zubkov, E. G. Goralski, S. D. Walck and J. T. Yates, *J. Phys. Chem. B*, 2004, **108**, 6004–6008.
20 S. H. Cheung, P. Nachimuthu, A. G. Joly, M. H. Engelhard, M. K. Bowman and S. A. Chambers, *Surf. Sci.*, 2007, **601**, 1754–1762.
21 S. H. Cheung, P. Nachimuthu, M. H. Engelhard, C. M. Wang and S. A. Chambers, *Surf. Sci.*, 2008, **602**, 133–141.
22 T. Ohsawa, I. Lyubinetsky, Y. Du, M. A. Henderson, V. Shutthanandan and S. A. Chambers, *Phys. Rev. B: Condens. Matter*, 2009, **79**, 7.
23 M. Batzill, E. H. Morales and U. Diebold, *Chem. Phys.*, 2007, **339**, 36–43.
24 N. Daude, C. Gout and C. Jouanin, *Phys. Rev. B: Solid State*, 1977, **15**, 3229–3235.
25 J. Tauc, R. Grigorov and A. Vancu, *Phys. Status Solidi*, 1966, **15**, 627–637.

26 D. C. Cronemeyer, *Phys. Rev.*, 1952, **87**, 876–886.
27 J. Graciani, J. F. Sanz and A. M. Marquez, *J. Phys. Chem. C*, 2009, **113**, 930–938.
28 M. Delfino, J. A. Fair and D. Hodul, *J. Appl. Phys.*, 1992, **71**, 6079–6085.
29 N. C. Saha and H. G. Tompkins, *J. Appl. Phys.*, 1992, **72**, 3072–3079.
30 A. Glaser, S. Surnev, F. P. Netzer, N. Fateh, G. A. Fontalvo and C. Mitterer, *Surf. Sci.*, 2007, **601**, 1153–1159.
31 I. Milosev, H. H. Strehblow and B. Navinsek, *Thin Solid Films*, 1997, **303**, 246–254.
32 H. Y. Chen, A. Nambu, W. Wen, J. Graciani, Z. Zhong, J. C. Hanson, E. Fujita and J. A. Rodriguez, *J. Phys. Chem. C*, 2007, **111**, 1366–1372.
33 M. Che and C. Naccache, *Chem. Phys. Lett.*, 1971, **8**, 45–48.
34 N. D. Shinn and K. L. Tsang, *presented at the 37th National Symposium of the American Vacuum Society, Toronto, Canada*, 1990.
35 J. R. Akse and H. B. Whitehurst, *J. Phys. Chem. Solids*, 1978, **39**, 457–465.
36 J. C. Fisher, *J. Appl. Phys.*, 1951, **22**, 74–77.
37 M. A. Henderson, *Surf. Sci.*, 1999, **419**, 174–187.
38 U. Diebold, *Surf. Sci. Rep.*, 2003, **48**, 53–229.
39 H. Iddir, S. Ogut, P. Zapol and N. D. Browning, *Phys. Rev. B: Condens. Matter*, 2007, **75**, 4.
40 M. V. Ganduglia-Pirovano, A. Hofmann and J. Sauer, *Surf. Sci. Rep.*, 2007, **62**, 219–270.
41 M. Li, W. Hebenstreit, U. Diebold, A. M. Tyryshkin, M. K. Bowman, G. G. Dunham and M. A. Henderson, *J. Phys. Chem. B*, 2000, **104**, 4944–4950.
42 M. A. Henderson, W. S. Epling, C. L. Perkins, C. H. F. Peden and U. Diebold, *J. Phys. Chem. B*, 1999, **103**, 5328–5337.